



ISTITUTO NAZIONALE DI RICERCA METROLOGICA Repository Istituzionale

Mathematical modeling for the design of evolution experiments to study the genetic instability of metabolically engineered photosynthetic microorganisms

This is the author's accepted version of the contribution published as:

Original

Mathematical modeling for the design of evolution experiments to study the genetic instability of metabolically engineered photosynthetic microorganisms / Battaglino, Beatrice; Arduino, Alessandro; Pagliano, Cristina. - In: ALGAL RESEARCH. - ISSN 2211-9264. - 52:(2020), p. 102093. [10.1016/j.algal.2020.102093]

Availability:

This version is available at: 11696/64012 since: 2020-12-23T09:23:40Z

Publisher:

Elsevier

Published

DOI:10.1016/j.algal.2020.102093

Terms of use:

This article is made available under terms and conditions as specified in the corresponding bibliographic description in the repository

Publisher copyright

(Article begins on next page)

Mathematical modeling for the design of evolution experiments to study the genetic instability of metabolically engineered photosynthetic microorganisms

Authors

Beatrice Battaglino^{a,\$}, Alessandro Arduino^{b,\$}, Cristina Pagliano^{a,*}

Author affiliation

^a Applied Science and Technology Department-BioSolar Lab, Politecnico di Torino, Environment Park,
Via Livorno 60, 10144 Torino, Italy

^b Istituto Nazionale di Ricerca Metrologica (INRiM), Strada delle Cacce 91, 10135 Torino, Italy

^{\$} contributed equally

* Correspondence should be addressed to: cristina.pagliano@polito.it

Published journal article available at DOI: <https://doi.org/10.1016/j.algal.2020.102093>

© 2020. This manuscript version is made available under the CC-BY-NC-ND 4.0 license
<http://creativecommons.org/licenses/by-nc-nd/4.0/>

Abstract

Engineering the metabolism of photosynthetic microorganisms with the aim of converting CO₂ and water, by exploiting solar energy, into end-products of commercial value is a rising interest in the biotechnology field. The producing host that carries a genetic modification not associated with competitive fitness advantage usually experiences a production burden (i.e., a metabolic burden related to product synthesis), leading to genetic instability and abortive production phenotype. The genetic instability of these engineered strains is a major hindrance to the spreading of large-scale photosynthetic cell factory processes. This genetic instability can be studied by means of evolution experiments, which are often time-consuming. In these experiments, the cell population is subjected to a long-term culturing during which the possible variation of the number of producers and of cells that lose the production traits, here defined as retro-mutants, is recorded. Here, a mathematical model that describes the dynamics of retro-mutants into a population of metabolically engineered photosynthetic microorganisms has been developed. The model has been used to simulate evolution experiments, conducted both in continuous (chemostat and turbidostat) and semi-continuous (serial batch transfer) culturing modes. These simulations allowed identifying the set of operative parameters for each cultivation mode that optimizes an evolution experiment in terms of experimental time needed to detect the arising of retro-mutants. Moreover, it has been found that in a scale of number of microbial generations only two parameters, precisely the production burden and the mutation rate, are determinant for the appearance of retro-mutants. These parameters are intrinsic features of any metabolically engineered strain and do not depend on the adopted cultivation system or on the microbial growth kinetics characteristics. This result further extends the applicability of the model also to non-photosynthetic metabolically engineered microorganisms.

Keywords: photosynthetic microorganisms, metabolic engineering, genetic instability, dynamic population models, biotechnology

1. Introduction

Photosynthetic cell factories, based on prokaryotic cyanobacteria and eukaryotic microalgae, are promising biotechnological platforms because of their capability of directly converting CO₂ and water, by exploiting solar energy, into end-products of commercial value, such as lipids, pigments, building blocks for polymer synthesis, and commodity chemicals [1–3]. Many proof-of-concept studies have been showcased [4–8] and many efforts have been made to increase the productivity of promising strains by means of metabolic engineering [9–13]. This consists in the use of different genetic engineering techniques to modify the metabolism of an organism by tuning specific metabolic pathways to trigger the targeted metabolite production [14]. To transform a wild-type microorganism in a producer of a specific metabolite of interest three strategies commonly used for manipulating the genome of the host microorganism are: (i) the over-expression of native genes to increase the production of compounds naturally occurring in the cell, (ii) the deletion of native genes to block competing metabolic pathways, and (iii) the insertion of heterologous genes for the heterologous synthesis of products. Notably, in the last decade a substantial contribution to this approach came from the increasing availability of fully sequenced genomes and genome scale metabolic models of many photosynthetic microorganisms [15–17].

The producing host carrying a genetic modification not associated with competitive fitness advantage usually experiences a production burden (i.e., a metabolic burden related to product synthesis), leading to genetic instability and degenerated/abortive production phenotype [18]. The genetic instability of the metabolically engineered strains nowadays remains one of the major constraints to the spreading of large-scale photosynthetic cell factory processes [19]. The loss of productivity and yield in several metabolically engineered photosynthetic microorganisms has been mainly associated to the arising inside the producers' population of retro-mutants [20–23], which are producing cells that lose their production capabilities by random mutation of the genes responsible for the formation of the target compound(s).

Indeed, the new trait(s) introduced into the producer cells can alter the carbon flux or interfere with the resource allocation inside the cell, often resulting in detrimental effects on the cell fitness [24]. This fitness impairment is determined by a production burden arising from the specific cost of the modified metabolic pathway in the producer cells, which can be exerted through the synthesis of additional DNA and protein molecules, depletion of essential endogenous compounds, and accumulation of toxic intermediates or by-products [24,25]. The entity of this production burden varies depending on the design and type of the modification to the biosynthetic pathway involved in the production of the target metabolite [26]. The retro-mutant cells, which have lost their production capabilities and are no longer affected by the production burden, have a fitness advantage compared to the producers and are subjected to a positive selection pressure that leads to their quick take-over of the culture. New approaches of metabolic engineering oriented at containing the genetic instability issue have been developed. One of the most promising strategies aims at aligning the target metabolite synthesis with the microbial fitness, so to reduce the probability of retro-mutation of the producing strain [27,28]. This metabolic engineering approach has been recently implemented in cyanobacterial cell factories [29,30]. Another recently proposed strategy consists in tying up the end-product with an intermediary metabolite that is essential to the growth of the producing host (i.e., metabolic addiction) and introducing feedback control genetic circuits conferring to the overproduction strain a competitive growth advantage (i.e., feedback genetic circuits) [31,32].

Evolution experiments are a common tool to assess how long an engineered strain will maintain its production capability [33]. During evolution experiments, microorganisms are subjected to long-term culturing under controlled conditions, either in continuous (chemostat, turbidostat) or semi-continuous (serial batch transfers) systems [33,34]. In this way, it is possible to detect the arising of retro-mutants with an expected increased fitness with respect to the producers and thus evaluate the instability of the engineered strain [35]. Evolution experiments are often time- and resource-consuming. Here we propose

a mathematical model describing the dynamics of retro-mutants in a population of photosynthetic microorganisms for the optimization of an evolution experiment carried out in chemostat, turbidostat and serial batch transfers systems. Precisely, the set of operative parameters that allows to detect in the shortest experimental time the arising of retro-mutants was identified for each cultivation system.

The presented mathematical model is suitable for describing the evolution dynamics of a metabolically engineered photosynthetic population, because it takes into account the intrinsic biological properties influencing its growth and evolution. Photosynthetic microorganisms are autotrophs for which the light is a major determinant of their photosynthetic activity and, consequently, their growth. Indeed, even under nutrient saturation conditions, their growth can be either inhibited, if light intensity exceeds the saturating light level necessary to guarantee the maximum photosynthetic rate thus causing photoinhibition, or limited, if light intensity is insufficient for the reverse effect. Inside a cultivation system, even under constant sustained incident light, the photosynthetic microbial cells can experience growth limitation, due to the light attenuation occurring at increased biomass concentrations. This is the so-called self-shading effect [36], which consists in the mutual shading of the cells occurring via scattering by the cells or via adsorption by the pigments. To describe the growth of photosynthetic microorganisms, many growth kinetic models have been proposed [37–39]. Among them, the simplest one derives from the adaptation of the Monod model [40], originally conceived to describe the growth of heterotrophic microorganisms, substituting a substrate-limited growth with a light-limited one [36]. More complex models accounting for multiple factors influencing the growth of photosynthetic microorganisms, such as the intrinsic biological features related to internalization of C, N, P nutrients, light, temperature, and physical properties of the cultivation system, have been devised [37–39,41]. Such detailed models are beyond the scope of this work. For this reason, in the present work a kinetic growth model has been adopted to account specifically for the effects of the light on the variation of the growth rate, considering both light-limitation and photoinhibition, [42]. This model has been applied to simulate

laboratory evolution experiments performed in different cultivation systems illuminated by constant continuous light. It is worth noting that the use of this light-dependent growth kinetic model is relevant to take into account the self-shading effect, occurring when the cell density increases.

When studying the genetic instability of a metabolically engineered strain by means of a microbial evolution experiment, the aim is to record the variation in the ratio between the producing population and the subpopulation(s) arising by random mutation. These experiments usually start from a monoclonal population with no recombinant capability, therefore, ideally homogeneous. In this situation, the only source of variability regards the spontaneous mutations arising in the population subjected to the natural selection [43]. Next generation sequencing technologies, together with innovative experimental procedures such as marker divergence analysis [44], allow detecting these mutations and gaining useful information about the dynamics of adaptation in microbial populations [45]. Besides the experimental realm, mathematical tools have been developed to model and virtually reproduce the appearance of random mutations and the consequent natural selection. Both deterministic [46–48] and stochastic [49–52] models present in literature highlighted that the relative fitness advantage of each mutant within the population plays a key role in the evolution dynamics. These models, when including a growth rate, considered it as constant. Here, we will adopt a model that includes a growth rate which can vary in a light-dependent manner. A plethora of models have been devised to take into account haploid populations (i.e., one copy of each gene per individual) as well as polyploid populations (i.e., more than one copy of each gene per individual), and asexually or sexually reproducing individuals [53]. Here, we will focus on modeling a haploid asexually reproducing photosynthetic population, in which only one type of mutation can occur (i.e., clonal interference, leading to competition between mutants carrying different beneficial variants in the population, is not present). However, it should be noted that many photosynthetic microorganisms, including several strains of cyanobacteria, show polyploidy [54]. The larger is the ploidy of the microorganism, the higher is the probability that mutations manifest themselves

at the phenotypic level [55]. Polyploidy is species-dependent and, within a species, varies with the growth phase and changing environmental factors (e.g., light intensity, phosphate concentration), making hard its quantification [56]. For this reason, it is difficult to accurately simulate the evolution dynamics of a polyploid system under varying growth and environmental conditions. Nevertheless, by assuming a constant probability of mutation for a polyploid population, our model can be used to describe the average behaviour of this population in an evolution experiment run under controlled conditions.

In this work, a novel deterministic model describing the dynamics of a producing population of photosynthetic individuals that is susceptible to mutational suppression is proposed. Firstly, the model was validated against the stochastic Moran model [51], which takes into account the random element of the onset of mutations in a population, and thus better represents the randomness of evolution dynamics. Secondly, the model, which includes a light-dependent variable growth rate, was applied to simulate an evolution experiment with the model cyanobacterium *Synechocystis* sp. PCC 6803 cultured in chemostat, turbidostat and serial batch transfer modes. Finally, once the values specific for the considered strain have been assigned to the model parameters, the proposed model was used to identify the optimal operative conditions for each cultivation system to perform an evolution experiment that guarantees to detect the appearance of retro-mutants in the shortest experimental time. In addition, this study showed that on a scale of number of microbial generations the arising of retro-mutants only depends on the mutation rate and the production burden of the engineered strain, irrespective of the microbial growth kinetics characteristics. This result further widens the applicability of the model also to non-photosynthetic metabolically engineered microorganisms.

2. Material and methods

2.1. Deterministic modeling

2.1.1. Growth and evolution model

To properly model the dynamics of an engineered producing microbial population, in which heterologous or extra copies of gene(s) have been inserted, at least two phenomenological observations must be considered. Firstly, the synthesis of a product can be burdensome for the producing population, whose growth rate is consequently negatively affected. Secondly, the probability of the arising of retro-mutants that lose the production trait is non-negligible, whereas the spontaneous development of the inserted trait is almost impossible in the short time-scale of laboratory experiments.

The evolution of the engineered population inside a culture volume can be modeled by the following system of ordinary differential equations (ODE) [57],

$$\begin{cases} \frac{dp}{dt} = \mu_p(1 - m)p - Dp \\ \frac{dw}{dt} = \mu_w w + \mu_p m p - Dw \end{cases}, \quad (1)$$

where $p(t)$ and $w(t)$ are, respectively, the producing and the retro-mutant biomass densities at time instant t , μ_p and μ_w are the growth rates of the producing and retro-mutant populations, respectively, m is the specific mutation rate of the considered strain and D is the possible dilution rate. It is worth noting that the producers can retro-mutate only if they are growing (i.e., $\mu_p > 0$).

The growth rates of the producing and retro-mutant strains are assumed to be related each other by means of a constant production burden ρ , which represents the additional metabolic cost required to the producing strain to carry out the synthesis of the target product. Namely, $\mu_p = \mu_w (1 - \rho)$. In the following, μ_w is assumed always greater than zero. The assumption of a constant production burden does not take into account the effects of fluctuating environmental conditions (pH, temperature, etc.) [58] and of toxic products potentially affecting differently the producers and the retro-mutants [59]. Since the simulations aim at reproducing a controlled laboratory experiment with expected limited environmental fluctuations, their effect on the production burden are not considered in the modelling. In addition, for the sake of simplicity, also specific cases, such as unpaired toxicity of the product in the producers and retro-mutants, are not considered in this context.

To adapt the system (1) to photosynthetic microorganisms, the growth rate μ_w has been modeled according to the Aiba model [42]. This model describes the growth rate in function of the light intensity taking into account the light-limitation, light-saturation and photoinhibition events as

$$\mu_w(I) = c_{max} \frac{I}{k_s + I + I^2/k_l} - k_d. \quad (2)$$

In the latter equation I is the incident light intensity, c_{max} is the maximum cell carbon uptake, k_s and k_l are the photo-saturation and inhibition constants, respectively, and k_d is the specific decay rate of the microorganism, accounting for maintenance, cell turnover/repair and carbon loss. For simplicity, no nutrient limiting factors, such as N, P or C, other than light are assumed; nonetheless, they can be easily added by multiplicative modeling [38]. This simplification does not affect the presented results.

The distribution of the light intensity I in the culture vessel, in general, is not homogeneous, because light is both absorbed and scattered through the culturing medium by the cells, which produce a self-shading effect [36]. Light extinction through the culture medium is modeled in first approximation by the Lambert-Beer law $I(z) = I_0 \exp(-\xi z)$, being I_0 the incident light intensity, ξ the extinction coefficient and z the length of the optical path. The extinction coefficient contains both the contribution of the background (e.g., culture medium, bubbles) and of the cell population, here modeled as

$$\xi = \xi_b + \varepsilon_p p + \varepsilon_w w, \quad (3)$$

where ξ_b is the extinction coefficient of the background and ε_p and ε_w are the specific extinction coefficient of the producing and retro-mutant populations, respectively.

The heterogeneity of the light intensity distribution within the reactor volume forces the adoption of averaging to describe the system evolution in terms of ODE. To this end, two limit approximations can be adopted: 1) if the mixing rate is assumed higher than the photosynthetic response to light in terms of growth rate variation (i.e., infinite mixing assumption), then the light intensity is averaged [39]; 2) if the photosynthetic response of the cells to light is significantly faster than the mixing rate, then the growth

rate itself is averaged [39]. In the simulations, the latter approach has been used. Thus, in equation (1), μ was substituted with its spatial average $\bar{\mu}$, computed as

$$\bar{\mu} = V^{-1} \int_V \mu(I(x)) dx, \quad (4)$$

where V is the volume of the cultivation system. It is worth noting that the spatial average growth rate is determined by the amount of light experienced by the cells in each point of the photobioreactor. For notation simplicity, hereafter the overbar is omitted.

The described deterministic model has been implemented in a Python 3 code.

2.1.2. Estimation of parameters assigned to the model

In this paper, the parameters of the growth and evolution model used in the simulations refer to *Synechocystis* sp. PCC 6803 (hereafter *Synechocystis*) and are summarized in **Table 1**.

Values assigned to the growth model parameters, reported in equations (2) and (3), are k_d , c_{max} , k_s , k_l and ε . The specific decay rate k_d of a photosynthetic microorganism is reasonably constant for any non-saturating light intensity and increases under inhibiting irradiation [60]. Since all the simulations were performed in non-saturating light conditions (i.e., up to $150 \mu\text{mol photons m}^{-2} \text{ s}^{-1}$), k_d was kept constant and equal to 0.0079 h^{-1} , a value reported for *Synechocystis* grown under similar light intensities [61]. For the parameters c_{max} , k_s and k_l , values were assigned by fitting the experimental data of growth rate and transmitted light intensities collected in *Synechocystis* at supplied light intensities ranging from limiting to photoinhibitory light conditions [62]. The specific extinction coefficient ε is subjected to dynamic changes due to the photoacclimation process by which photosynthetic cells modulate their pigment content in response to varying light intensity [63,64]. A modeling approach to describe its dynamic variations has been proposed [65,66]. In this study, however, photoacclimation has not been considered and a constant specific extinction coefficient ε , equal for producer and retro-mutant populations

($\varepsilon_p = \varepsilon_w = \varepsilon$), was used, assigning a value of $0.16 \text{ m}^2 \text{ g}^{-1}$ as reported for light intensities similar to those of our simulations [67]. Moreover, in equation (3) the turbidity of the background has been neglected by setting $\zeta_b = 0$.

Values assigned to the evolution model reported in equation (1) are m and ρ . The mutation rate m , which represents the bacterial genomic mutation rate that generates beneficial mutations, has been estimated in the range of 10^{-8} - 10^{-5} per generation in different microorganisms [68]. In this study, it was set equal to 10^{-5} per generation according to [69]. The production burden ρ tested in the simulations was set equal to 15 % and 30 %. These are realistic values of production burden in the range of those shown by metabolically engineered microorganisms, either cyanobacteria or heterotrophic bacteria [21,23,48,70], which can be estimated as the ratio between the growth rate of the producer and that of the retro-mutant, assumed to retrieve the wild-type growth phenotype.

2.1.3. Cultivation modes and culture vessel geometries

Three different cultivation modes have been investigated in the simulations: chemostat, turbidostat and serial batch transfer.

A chemostat is a continuous cultivation mode in which the culture volume is kept constant by means of an outlet volumetric flow determining the continuous removal of broth culture and an inlet volumetric flow introducing fresh medium in the reactor, both working at the same rate. In the chemostat simulations, the dilution rate D in equation (1) assumes a positive and constant value. For values of D higher than the maximum growth rate possible for the cells under the supplied irradiance, the chemostat mode leads to the wash-out of the culture from the reactor; otherwise, the system tends to a steady state in which the growth rate of the cell population is equal to D . By setting in equation (1) the dilution rate $D = 0$, the particular case of a batch cultivation mode in principle could be simulated. In batch mode, all resources are provided in finite amount at the beginning of the cultivation with the exception of light. In the model,

however, nutrient depletion is not included, thus the growth can be described only as long as the resources different from light are not in limiting concentrations. Since a nutrient saturating condition cannot be assured indefinitely, this cultivation mode has not been simulated in the present study.

In turbidostat mode, fresh medium is supplied to the culture and dilutions are performed according to optical density (OD) measurements, with the aim of keeping almost constant the OD of the culture. To simulate this process, two OD values are set, namely a base value (OD_b) and a cut-off value (OD_c). At the end of each time interval of a certain duration T , the OD is measured and if its value is greater than OD_c , then a dilution with fresh medium is performed to restore the OD_b . Mathematically, this process can be modeled by introducing in equation (1) a time-varying D ; however, from a computational point of view, it is more convenient to set $D = 0$ and assume an instantaneous dilution.

A serial batch transfer consists of the repeated inoculation of the growing culture in fresh medium for many rounds of cultivation. In experimental practice, this mode is performed manually in flasks by transferring part of a batch culture in new cultivation medium. A serial batch transfer can be considered as a special case of turbidostat, with the only difference of a longer duration of the time interval between two successive dilutions; from the computational point of view, there are no differences between these two modes.

In the simulations, for all the cultivation modes a continuous supply of light was assumed. Moreover, in the turbidostat and serial batch transfer simulations, a fixed value of 0.8 was used for OD_c .

Each cultivation mode has been first associated to the vessel geometry most commonly used to perform a laboratory evolution experiment [33]. For chemostat and turbidostat modes, a flat panel of thickness 3.70 cm laterally-illuminated by a far light source with $150 \mu\text{mol photons m}^{-2} \text{s}^{-1}$ has been considered (**Figure S1a**). For serial batch transfers, a 100 mL Erlenmeyer flask filled with 20 mL of culture and top-illuminated by a far light source with $30 \mu\text{mol photons m}^{-2} \text{s}^{-1}$ has been used (**Figure S1b**). Details on

how to compute the average growth rate (4) for the considered vessel geometries are provided in Supplementary material (**Appendix A**).

2.2. Stochastic modeling

A stochastic process, whose behaviour recalls the random nature of the onset of mutations, can be used to describe the evolution dynamics, as an alternative to the deterministic model described above.

The Moran model is one of the simplest stochastic models proposed to describe the spontaneous appearance of mono-allelic mutants in a population [51]. The Moran model assumes a population size maintained constant and equal to N individuals. The discrete stochastic process at its basis provides the number of retro-mutants in the population at certain time instants. It is obtained by iterating the elementary Moran step, which advances in time for a fraction of a generation equal to $(\log(N+1) - \log(N)) / \log(2)$ and consists of two phases: first, one individual of the population is selected for duplication; then, one individual is selected to be removed.

In presence of a production burden, impaired probabilities are used to select the duplicating individual according to

$$P(\text{duplicating producer}) = \frac{p}{N + sw}, \quad P(\text{duplicating retro-mutant}) = \frac{(1 + s)w}{N + sw}, \quad (5)$$

where $P(E)$ is the probability that the generic event E is verified, p and w are the number of producers and retro-mutants in the population, respectively, and s is the selective advantage of the retro-mutants with respect to the producers. The latter is related to the production burden ρ , introduced in (1), by $s = \rho / (1 - \rho)$. If the individual selected for duplication is a retro-mutant, then its offspring will be a retro-mutant, too; otherwise, it may be a retro-mutant with probability $m * \log(2)$, i.e. the mutation rate, introduced in (1), in a scale of number of microbial generations. On the other hand, all individuals have the same uniform probability of being selected to be removed.

The values for the model parameters m and ρ have been assigned as described for the deterministic model (**Table 1**). The Moran model has been implemented in a C++ code.

3. Results and Discussion

3.1. Validation of the deterministic model

The output of a deterministic model is completely determined by the values assigned to its parameters and the initial conditions, and is representative of the average behaviour of a population. On the other hand, the output of a stochastic process is affected by the presence of a randomness source. This means that the same set of parameters and initial conditions will lead, in principle, to different output at each execution of the stochastic model better reproducing the variability of the biological system.

Despite requiring more input parameters, the adoption of the deterministic model has remarkable advantages with respect to the stochastic approach [71]. Indeed, it is significantly faster to be simulated, especially with large populations [72], and provides results of evolution dynamics in a temporal scale, whereas the stochastic model only in terms of number of generations occurred. This is due to the fact that the stochastic model only contains two biological parameters (i.e., the mutation rate and the fitness advantage) and cannot be further tailored on a specific strain, differently from the deterministic model. Given the advantages of the deterministic model, it has been validated against the stochastic one to assess its suitability to describe the evolution dynamics. To this aim, simulations were performed with the two methods and results of the trends of percentage of producers r , defined by

$$r = \frac{p}{p + w} 100 \%, \quad (6)$$

were compared (**Figure 1**).

First, it has been verified whether the output of the stochastic simulations has a deterministic behaviour by testing different values of population size (N), ranging from 10^5 to 10^8 individuals (**Figure 1a**). From

this analysis, it was evident that the random nature of the mutations outcome becomes relevant only for small populations (i.e., $N < 10^7$), as indicated by the larger variability of the output with both production burdens of 15 % and 30 % (**Figure 1a**). Thus, the system shows a deterministic behaviour when the population size is sufficiently large, a requirement easily satisfied in common operative conditions (e.g., for a *Synechocystis* culture, $0.25 \text{ OD}_{730} = 10^8$ cells per ml [73]). Secondly, the trend of the percentage of producers has been simulated with both the stochastic and the deterministic models setting N equal to 10^8 individuals, and the results were compared in a scale of number of generations of producers (calculated as shown in Supplementary Material, **Appendix B** and **Appendix C**) (**Figure 1b**). The comparison shows a complete overlapping between the results obtained with the two approaches for both values of ρ , confirming that the deterministic model perfectly describes the dynamics of retro-mutant appearance inside a sufficiently large population.

The validated deterministic model was used in all the following simulations.

3.2. Dynamic simulations of evolution experiments

In all the simulations, the percentage of producers r was computed for the entire duration of the evolution experiment, 80 days for chemostat, 60 days for turbidostat and 120 days for serial batch transfer. The temporal evolutions of a culture system in different cultivation modes were simulated assuming that no retro-mutants were originally present in the culture (i.e., $r(0) = 100 \%$) and that the initial producers biomass density $p(0)$ was such that the initial OD is equal to 0.1. The OD value was converted to the biomass density by using the conversion factor of $148 \text{ mg/L/OD}_{730}$, according to [74]. The results are reported in day time-scale.

3.2.1. Chemostat

The chemostat simulations were performed by testing increasing values of D from 0.01 h^{-1} to 0.07 h^{-1} (**Figure 2**). The trends of biomass density obtained with $\rho = 15 \%$ (**Figure 2a**) show that the producing population reaches in few days a first, temporary steady state. During this steady state, the producers' growth rate μ_p is equal to D and its biomass density p remains almost constant. This state, at a certain point, is perturbed by the appearance of retro-mutants (**Figure 2a**), which, by virtue of their fitness advantage, take over the culture and lead to a new, stable steady state. When this occurs, the producing population is depleted and the retro-mutant population keeps a constant biomass density w , such that its growth rate μ_w is equal to D . The disruption of the first apparent steady state happens sooner at higher values of D (**Figure 2a**) and is reflected in the faster reduction of the percentage of producers reported in **Figure 2b**. In particular, within the time-frame of the simulation, the instability does not appear with $D = 0.01 \text{ h}^{-1}$, whereas it leads to about 80 % reduction of the producers with $D = 0.03 \text{ h}^{-1}$ and an almost complete loss of producers with higher values of D by the end of the simulation (**Figure 2b**).

Figure 2c and **2d** show analogous trends for $\rho = 30 \%$. With this higher production burden it is more evident that for $D > 0.03 \text{ h}^{-1}$ the first temporary steady state of the producer population reaches a lower biomass density with respect to that reached by the retro-mutants at the following steady state (**Figure 2c**). Nevertheless, at these two steady states the growth rates of the producers and retro-mutants are the same and equal to D . The higher biomass of the steady state of the retro-mutants relies on the higher capacity of this sub-population to attenuate the self-shading effect with respect to the producer population, which, suffering from a metabolic production burden affecting negatively this capacity, at steady state reaches the same growth rate of the retro-mutants but at lower biomass. Moreover, with $\rho = 30 \%$ the instability of the producer population (**Figure 2d**) shows up faster than with $\rho = 15 \%$, and at the end of the simulations already with $D = 0.03 \text{ h}^{-1}$ the producers completely disappear from the culture.

3.2.2. Turbidostat and serial batch transfer

Both the turbidostat and the serial batch transfer cultivation modes are systems in which the culture experiences repeated dilutions. To assess the impact of the operative parameters adopted for the dilution process on the outcome of an evolution experiment, simulations were performed testing different values of interval duration between two consecutive OD checks (T) and base OD (OD_b) (**Figure 3**). Precisely, for the parameter T , values of 0.1 h, 0.5 h, 1 h and 6 h for turbidostat and of 24 h, 48 h, 72 h and 96 h for serial batch transfer were tested in the simulations. For the parameter OD_b , for both cultivation modes, values in the range between 0.2 and 0.7 were tested, that are respectively close to the initial and the cut-off OD values set in the simulations (see Methods section 2.1.3).

In the simulations of the turbidostat and serial batch transfer cultivation modes, the biomass and the growth rate of the population varied during the interval duration between two consecutive dilutions, depending on the operative parameters set (**Table S1**). This variation ranged between a minimum value of biomass, corresponding to the maximum growth rate observed immediately after each dilution (i.e., cells are in exponential growth phase), and a maximum value of biomass, corresponding to the minimum growth rate observed just before the dilution.

In the simulations of the turbidostat mode, a negligible dependence of the variation of the trend of the percentage of producers with respect to T was observed for both values of ρ (**Figure 3a**) and only for $\rho = 15\%$ and $OD_b = 0.7$ a slight delay of few days appeared between the trends computed with T of 1 h and 6 h. In this cultivation mode, the OD_b exerted a slightly higher effect on the appearance of retro-mutants, which was slightly faster (**Figure 3b**). However, varying the OD_b , the estimated delays in retro-mutants appearance was limited to few days, and in general, the lower was the OD_b value, the sooner the percentage of producers decreased within the population (**Figure 3b**). When comparing results of the simulations with $\rho = 15\%$ and $\rho = 30\%$, the impact of varying either T or OD_b on the trend of the

percentage of producers was always higher at lower production burden, and in general for both operative parameters a retarded appearance of retro-mutants occurred for $\rho = 15\%$ compared to $\rho = 30\%$.

The simulations of the serial batch transfer cultivation mode (**Figure 3c** and **3d**) showed a slower decrease of the percentage of producers with respect to the turbidostat mode (**Figure 3a** and **3b**) when comparing the same operative parameters and production burden. In this cultivation mode, both T (**Figure 3c**) and OD_b (**Figure 3d**) had a significant impact on the evolution of the producer population. In particular, low values of T (**Figure 3c**) as well as low values of OD_b (**Figure 3d**) induced a faster appearance of the retro-mutants. Analogously to the turbidostat, also in serial batch transfer cultivation mode the variation between the different trends of percentage of producers was larger with a lower production burden.

3.3. Comparison between cultivation systems

To select the best operative conditions to perform an evolution experiment aiming at detecting the appearance of retro-mutants in the shortest time in the different cultivation modes, we compared the results of all the simulations by looking at the time-instant at which the percentage of producers is reduced to the 50 % of the population. Indeed, this time-instant, hereafter referred to as $t_{50\%}$, is indicative of a remarkable instability in the producing strain at a certain time of the evolution experiment. Comparison of $t_{50\%}$ for the different cultivation modes is reported in **Figure 4**. In general, it is evident that, irrespective of the cultivation system, the higher is the production burden of the producing strain, the smaller is $t_{50\%}$. In the chemostat cultivation mode, $t_{50\%}$ decreased with increasing values of D (**Figure 4a**), and thus with increasing growth rates at steady state. For D between 0.03 h^{-1} and 0.07 h^{-1} , $t_{50\%}$ varied from about 70 to 30 days for $\rho = 15\%$ and from 29 to 14 days for $\rho = 30\%$, showing a two-fold difference between the two production burdens. The same difference is evident in the results for turbidostat and serial batch transfer cultivation modes (**Figure 4b** and **Figure 4c**). The turbidostat mode

was barely affected by the variation of T (**Figure 4b**) and OD_b (**Figure 4c**) in the range of values adopted for the simulations. Moreover, the chemostat operated with $D = 0.07 \text{ h}^{-1}$ (**Figure 4a**) and the turbidostat in all the simulated operative conditions (**Figure 4b** and **Figure 4c**) showed similar $t_{50\%}$ for both production burdens (i.e., $t_{50\%}$ of about 14 and 30 days respectively for $\rho = 30 \%$ and 15% in the chemostat and of about 15 and 27 days respectively for $\rho = 30 \%$ and 15% in the turbidostat). Indeed, in the turbidostat simulations, for all the OD_b and T tested, the growth rate oscillated around 0.07 h^{-1} (**Table S1**), that is the growth rate at stationarity of the chemostat with $D = 0.07 \text{ h}^{-1}$ (**Figure 4a**). Thus, considering this specific case, the two cultivation modes led to almost equivalent output of population dynamics.

On the other hand, the serial batch transfer resulted very sensitive to the variation of the operative parameters T and OD_b and $t_{50\%}$ occurred always later compared to the turbidostat mode (**Figure 4b** and **Figure 4c**). Moreover, the variation of $t_{50\%}$ at different OD_b (shade areas in **Figure 4b**) and T (shade areas in **Figure 4c**) was always almost double for $\rho = 15 \%$ with respect to $\rho = 30 \%$ (i.e., at varying either T or OD_b , $t_{50\%}$ always ranged from about 70 to 87 days for $\rho = 15 \%$, and from about 38 to 45 days for $\rho = 30 \%$). Working at a small enough T (e.g., 24 h, **Figure 4b**), the dependence of $t_{50\%}$ on OD_b was limited; similarly, working at a sufficiently low OD_b (e.g., 0.2, **Figure 4c**), $t_{50\%}$ appeared to be slightly dependent on T . The operative parameters T and OD_b set respectively to 24 h and 0.2 (**Figure 4b** and **Figure 4c**) provided the conditions to observe the shortest $t_{50\%}$ (i.e., about 70 and 40 days for $\rho = 15 \%$ and 30% , respectively) in the serial batch cultivation mode. In the case of $\rho = 15 \%$, these conditions for serial batch transfer led to a $t_{50\%}$ similar to that of a chemostat operated with a $D = 0.03 \text{ h}^{-1}$ (**Figure 4a**). This reflects the similar growth rate experienced by the cultures in the two cultivation modes under these operative conditions (**Table S1** and **Figure 4a**). It is worth noting that T is the duration of the time interval between two consecutive checks and, therefore might not correspond to the interval between two dilution operations. This fact can be appreciated in the case of $\rho = 15 \%$ and OD_b 0.2 where the same $t_{50\%}$ was

observed using either T of 24 h, when a dilution every two checks occurs, or T of 48 h, when a dilution every check occurs (**Figure 4b**). These evidences are of interest to optimize the design of an evolution experiment in repeated batch transfer mode. Indeed, this is a very common technique for evolution experiments, due to its low cost and easiness of implementation in any laboratory, but it suffers from the possibility to perform the sampling due to the constrain of manual performance. Therefore, the outcome of the simulations provides useful indications about the operative conditions of OD_b that allow accomplishing the evolution experiment in the shortest time using a time interval T compatible with a manual repeated batch transfer experiment.

3.4. Roles of the mutation rate and the production burden in the population dynamics

In general, the results of the simulations suggest that, given a certain value of production burden, the reduction of the percentage of producers within the population is accelerated when cells experience high growth rates in the cultivation system. Indeed, when using the chemostat, the loss of the producer phenotype is faster working at the highest D not causing wash-out, which corresponds to the highest growth rate at steady state (**Figure 4a**). Conversely, in case of the turbidostat and serial batch transfer modes frequent or large dilutions, avoiding a long permanence of cells in the slow non-exponential growth phase responsible for lower growth rates (**Table S1**), induce a faster loss of the producer phenotype.

To understand the relationship observed in the simulations between the growth rate of the producer population and the trend of the percentage of producers r , it is convenient to convert the trend of r from the day time-scale into a scale of number of microbial generations of producers. By doing this (see Supplementary Materials **Appendix B** for the complete mathematical demonstration), it is evident that the trend of the percentage of producers depends exclusively on the parameters ρ and m , irrespective of the cultivation mode adopted. Consequently, once the producing strain is characterized in terms of

production burden and mutation rate, it is possible to evaluate the number of generations of producers after which the percentage of producers drops to 50 %, designated as $g_{p,50\%}$, which is independent of the cultivation mode adopted in the evolution experiment. For an optimal design of the evolution experiment, maximizing the elapsing of generations per day will minimize the $t_{50\%}$ at which the appearance of a substantial number of retro-mutants is observed.

Figure 5 shows the counting of generations of producers for the operative conditions that minimize the $t_{50\%}$ of evolution experiments performed in the different cultivation modes, which are respectively $D = 0.07 \text{ h}^{-1}$ for chemostat, $T = 0.1 \text{ h}$ and $\text{OD}_b = 0.2$ for turbidostat and $T = 24 \text{ h}$ and $\text{OD}_b = 0.2$ for serial batch transfer, as deduced from **Figure 4**. In our simulations, the critical generation $g_{p,50\%}$ corresponded to the generation number 39 for $\rho = 30 \%$ and 80 for $\rho = 15 \%$ and occurred at diverse time instant $t_{50\%}$ for each cultivation mode (**Figure 5**), since the growth rate of the culture changes according to the cultivation system. In **Figure 5**, the values of $t_{50\%}$ can be retrieved from the intersection between the generation counting curves of each cultivation mode and the horizontal lines indicating the $g_{p,50\%}$. The generation counting in the chemostat and turbidostat modes was almost the same during the first 20 days for $\rho = 30 \%$, whereas it was slightly different since the beginning for $\rho = 15 \%$. On the other hand, the generation counting in the serial batch transfer was slower with respect to the chemostat and turbidostat modes. In **Figure 5**, the different slope of the generation counting curves is proportional to the averaged growth rate of the producers in the different cultivation modes. Therefore, it is evident that, for a given value of production burden, the higher is the growth rate during the evolution experiment, the sooner the instability of the engineered strain will show up.

The trend of the percentage of producers in a scale of number of microbial generations, as well as the value of $g_{p,50\%}$, is completely determined by the parameters ρ and m . The influence of ρ has been deeply discussed in the simulations above, testing values equal to 15 % and 30 %. We extended this investigation also to the influence of m , comparing simulation results obtained setting values equal to 10^{-8} and 10^{-5} per

generation (**Figure S2**), two limit mutation rates reported in literature for different microorganisms [68]. Given a fixed value of m , higher values of the production burden ρ determine a decrease of producers at a lower number of generations characterized by a higher velocity of their disappearance (**Figure S2**). On the other hand, given a fixed value of ρ , higher values of the mutation rate m determine a decrease of producers at a lower number of generations, without altering the velocity of this decrease (**Figure S2**).

4. Conclusions

In the laboratory practice, evolution experiments to check the genetic instability of metabolically engineered microorganisms are often time-consuming. To identify the optimal set of operative conditions that minimizes the experimental time required for an evolution experiment suited for metabolically engineered photosynthetic microorganisms, a novel mathematical model has been developed and used to simulate the dynamics of retro-mutants appearance in three common cultivation modes (chemostat, turbidostat and serial batch transfer). This model has been tailored to specifically take into account the variation of the growth rate in dependence of the light intensity experienced by the photosynthetic microorganisms, considering both the light effects of self-shading and photoinhibition. In general, the simulations showed that, in each cultivation system, the appearance of retro-mutants is faster when operative parameters that guarantee high growth rates are adopted. The identification of these parameters allows the fine-tuning of the cultivation set up to reduce the time duration of an evolution experiment. The analysis of the model revealed that, when assuming a linear relationship between the growth rates of producers and retro-mutants by means of a constant production burden (i.e., $\mu_p = \mu_w (1 - \rho)$), the appearance of retro-mutants in a scale of number of microbial generations depends exclusively on the production burden and the mutation rate and is independent of cultivation mode and operative conditions. It is worth saying that this result holds even when other factors than photoinhibition and self-shading are considered. Indeed, since the trend of the percentage of producers expressed in a scale of number of

microbial generations is affected only by these two parameters, other growing conditions characterized by limiting substrates, photoacclimation and other complex phenomena can be easily investigated within the same mathematical framework here proposed. Conversely, a case-by-case investigation is required if the relation between the growth rates of producers and retro-mutants is non-linear, for instance when the production burden and the mutation rate are influenced by fluctuating factors, such as variable environmental conditions. Hence, the mathematical model here proposed will be seminal for future in-depth analysis of more complex relations existing between the growth rates of the producers and retro-mutants in long-term evolution experiments. Moreover, the proposed model could be used to describe other experimental procedures involving the arising of spontaneous mutations, such as the adaptive laboratory evolution used to select microorganisms accumulating beneficial mutations [75].

Author Contributions

B.B. first conceived the study. A.A. and C.P. assisted B.B. in designing the analyses. A.A. and B.B. developed the mathematical framework. A.A. wrote the software. A.A. and B.B. performed the simulations. A.A., B.B. and C.P. analysed the data. C.P. supervised the study. B.B. drafted the manuscript. A.A. and C.P. critically revised the manuscript. All the authors approved the final manuscript.

Conflict of interest statement

The authors declare that the research was conducted in the absence of any commercial or financial relationship that could be construed as a potential conflict of interests.

Acknowledgements

The authors would like to thank Prof. Alberto Bertucco and Dr. Eleonora Sforza from Università di Padova for useful discussions.

Statement of informed consent, human/animal rights

No conflicts, informed consent, or human or animal rights are applicable to this study.

Supplementary data

Supplementary data to this article: Appendix A, Appendix B, Appendix C, Figure S1, Figure S2, Table S1.

References

- [1] R.H. Wijffels, O. Kruse, K.J. Hellingwerf, Potential of industrial biotechnology with cyanobacteria and eukaryotic microalgae, *Curr. Opin. Biotechnol.* 24 (2013) 405–413. <https://doi.org/10.1016/j.copbio.2013.04.004>.
- [2] M. Koller, A. Muhr, G. Braunegg, Microalgae as versatile cellular factories for valued products, *Algal Res.* 6 (2014) 52–63. <https://doi.org/10.1016/j.algal.2014.09.002>.
- [3] D. Gangl, J.A.Z. Zedler, P.D. Rajakumar, E.M.R. Martinez, A. Riseley, A. Włodarczyk, S. Purton, Y. Sakuragi, C.J. Howe, P.E. Jensen, C. Robinson, Biotechnological exploitation of microalgae, *J. Exp. Bot.* 66 (2015) 6975–6990. <https://doi.org/10.1093/jxb/erv426>.
- [4] P. Lindberg, S. Park, A. Melis, Engineering a platform for photosynthetic isoprene production in cyanobacteria, using *Synechocystis* as the model organism, *Metab. Eng.* 12 (2010) 70–79. <https://doi.org/10.1016/j.ymben.2009.10.001>.
- [5] Z. Gao, H. Zhao, Z. Li, X. Tan, X. Lu, Photosynthetic production of ethanol from carbon dioxide

in genetically engineered cyanobacteria, *Energy Environ. Sci.* 5 (2012) 9857–9865.

<https://doi.org/10.1039/c2ee22675h>.

- [6] P.E. Savakis, S.A. Angermayr, K.J. Hellingwerf, Synthesis of 2,3-butanediol by *Synechocystis* sp. PCC6803 via heterologous expression of a catabolic pathway from lactic acid- and enterobacteria, *Metab. Eng.* 20 (2013) 121–130. <https://doi.org/10.1016/j.ymben.2013.09.008>.
- [7] X. Liu, R. Miao, P. Lindberg, P. Lindblad, Modular engineering for efficient photosynthetic biosynthesis of 1-butanol from CO₂ in cyanobacteria, *Energy Environ. Sci.* 12 (2019) 2765–2777. <https://doi.org/10.1039/c9ee01214a>.
- [8] X.M. Sun, L.J. Ren, Q.Y. Zhao, X.J. Ji, H. Huang, Enhancement of lipid accumulation in microalgae by metabolic engineering, *Biochim. Biophys. Acta - Mol. Cell Biol. Lipids.* 1864 (2019) 552–566. <https://doi.org/10.1016/j.bbalip.2018.10.004>.
- [9] J.W.K. Oliver, S. Atsumi, Metabolic design for cyanobacterial chemical synthesis, *Photosynth. Res.* 120 (2014) 249–261. <https://doi.org/10.1007/s11120-014-9997-4>.
- [10] S.A. Angermayr, A. Gorchs Rovira, K.J. Hellingwerf, Metabolic engineering of cyanobacteria for the synthesis of commodity products, *Trends Biotechnol.* 33 (2015) 352–361. <https://doi.org/10.1016/j.tibtech.2015.03.009>.
- [11] C. Banerjee, K.K. Dubey, P. Shukla, Metabolic engineering of microalgal based biofuel production: Prospects and challenges, *Front. Microbiol.* 7 (2016). <https://doi.org/10.3389/fmicb.2016.00432>.
- [12] P. Lindblad, D. Fuente, F. Borbe, B. Cicchi, J.A. Conejero, N. Couto, H. Čelešnik, M.M. Diano, M. Dolinar, S. Esposito, C. Evans, E.A. Ferreira, J. Keller, N. Khanna, G. Kind, A. Landels, L. Lemus, J. Noirel, S. Ocklenburg, P. Oliveira, C.C. Pacheco, J.L. Parker, J. Pereira, T.K. Pham, F. Pinto, S. Rexroth, M. Rögner, H.J. Schmitz, A.M.S. Benavides, M. Siurana, P. Tamagnini, E. Touloupakis, G. Torzillo, J.F. Urchueguía, A. Wegelius, K. Wiegand, P.C. Wright, M. Wutschel,

- R. Wünschiers, CyanoFactory, a European consortium to develop technologies needed to advance cyanobacteria as chassis for production of chemicals and fuels, *Algal Res.* 41 (2019) 101510. <https://doi.org/10.1016/j.algal.2019.101510>.
- [13] C.F. Muñoz, M.H.J. Sturme, S. D'Adamo, R.A. Weusthuis, R.H. Wijffels, Stable transformation of the green algae *Acutodesmus obliquus* and *Neochloris oleoabundans* based on *E. coli* conjugation, *Algal Res.* 39 (2019) 101435. <https://doi.org/10.1016/j.algal.2019.101435>.
- [14] D. Julleson, F. David, B. Pfleger, J. Nielsen, Impact of synthetic biology and metabolic engineering on industrial production of fine chemicals, *Biotechnol. Adv.* 33 (2015) 1395–1402. <https://doi.org/10.1016/j.biotechadv.2015.02.011>.
- [15] J. Nogales, S. Gudmundsson, I. Thiele, Toward systems metabolic engineering in cyanobacteria: Opportunities and bottlenecks, *Bioengineered.* 4 (2013) 158–163. <https://doi.org/10.4161/bioe.22792>.
- [16] T. Fujisawa, R. Narikawa, S.I. Maeda, S. Watanabe, Y. Kanesaki, K. Kobayashi, J. Nomata, M. Hanaoka, M. Watanabe, S. Ehira, E. Suzuki, K. Awai, Y. Nakamura, CyanoBase: A large-scale update on its 20th anniversary, *Nucleic Acids Res.* 45 (2017) D551–D554. <https://doi.org/10.1093/nar/gkw1131>.
- [17] M. Aite, M. Chevallier, C. Frioux, C. Trottier, J. Got, M.P. Cortés, S.N. Mendoza, G. Carrier, O. Dameron, N. Guillaudeau, M. Latorre, N. Loira, G. V. Markov, A. Maass, A. Siegel, Traceability, reproducibility and wiki-exploration for “à-la-carte” reconstructions of genome-scale metabolic models, *PLoS Comput. Biol.* 14 (2018) 1–25. <https://doi.org/10.1371/journal.pcbi.1006146>.
- [18] G. Wu, Q. Yan, J.A. Jones, Y.J. Tang, S.S. Fong, M.A.G. Koffas, Metabolic Burden : Cornerstones in Synthetic Biology and Metabolic Engineering Applications, *Trends Biotechnol.* 34 (2016) 652–664. <https://doi.org/10.1016/j.tibtech.2016.02.010>.
- [19] P.R. Jones, Genetic instability in cyanobacteria - An elephant in the room?, *Front. Bioeng.*

- Biotechnol. 2 (2014) 1–5. <https://doi.org/10.3389/fbioe.2014.00012>.
- [20] J.H. Jacobsen, N.U. Frigaard, Engineering of photosynthetic mannitol biosynthesis from CO₂ in a cyanobacterium, *Metab. Eng.* 21 (2014) 60–70. <https://doi.org/10.1016/j.ymben.2013.11.004>.
- [21] W. Du, S.A. Angermayr, J.A. Jongbloets, D. Molenaar, H. Bachmann, K.J. Hellingwerf, F. Branco Dos Santos, Nonhierarchical Flux Regulation Exposes the Fitness Burden Associated with Lactate Production in *Synechocystis* sp. PCC6803, *ACS Synth. Biol.* 6 (2017) 395–401. <https://doi.org/10.1021/acssynbio.6b00235>.
- [22] I.S. Yunus, P.R. Jones, Photosynthesis-dependent biosynthesis of medium chain-length fatty acids and alcohols, *Metab. Eng.* 49 (2018) 59–68. <https://doi.org/10.1016/j.ymben.2018.07.015>.
- [23] K. Takahama, M. Matsuoka, K. Nagahama, T. Ogawa, Construction and analysis of a recombinant cyanobacterium expressing a chromosomally inserted gene for an ethylene-forming enzyme at the *psbAI* locus, *J. Biosci. Bioeng.* 95 (2003) 302–305. <https://doi.org/10.1263/jbb.95.302>.
- [24] B.R. Glick, Metabolic load and heterologous gene expression, *Biotechnol. Adv.* 13 (1995) 247–261. [https://doi.org/10.1016/0734-9750\(95\)00004-A](https://doi.org/10.1016/0734-9750(95)00004-A).
- [25] I. Shachrai, A. Zaslaver, U. Alon, E. Dekel, Cost of Unneeded Proteins in *E. coli* Is Reduced after Several Generations in Exponential Growth, *Mol. Cell.* 38 (2010) 758–767. <https://doi.org/10.1016/j.molcel.2010.04.015>.
- [26] O. Borkowski, F. Ceroni, G.B. Stan, T. Ellis, Overloaded and stressed: whole-cell considerations for bacterial synthetic biology, *Curr. Opin. Microbiol.* 33 (2016) 123–130. <https://doi.org/10.1016/j.mib.2016.07.009>.
- [27] S. Klamt, R. Mahadevan, On the feasibility of growth-coupled product synthesis in microbial strains, *Metab. Eng.* 30 (2015) 166–178. <https://doi.org/10.1016/j.ymben.2015.05.006>.
- [28] P. Jouhten, J. Huerta-Cepas, P. Bork, K.R. Patil, Metabolic anchor reactions for robust

- biorefining, *Metab. Eng.* 40 (2017) 1–4. <https://doi.org/10.1016/j.ymben.2017.02.010>.
- [29] W. Du, J.A. Jongbloets, C. Van Boxtel, H. Pineda Hernández, D. Lips, B.G. Oliver, K.J. Hellingwerf, F. Branco Dos Santos, Alignment of microbial fitness with engineered product formation: Obligatory coupling between acetate production and photoautotrophic growth, *Biotechnol. Biofuels*. 11 (2018) 38. <https://doi.org/10.1186/s13068-018-1037-8>.
- [30] W. Du, J.A. Jongbloets, M. Guillaume, B. Van De Putte, B. Battaglino, K.J. Hellingwerf, F. Branco Dos Santos, Exploiting Day- And Night-Time Metabolism of *Synechocystis* sp. PCC 6803 for Fitness-Coupled Fumarate Production around the Clock, *ACS Synth. Biol.* 8 (2019) 2263–2269. <https://doi.org/10.1021/acssynbio.9b00289>.
- [31] Y. Lv, S. Qian, G. Du, J. Chen, J. Zhou, P. Xu, Coupling feedback genetic circuits with growth phenotype for dynamic population control and intelligent bioproduction, *Metab. Eng.* 54 (2019) 109–116. <https://doi.org/10.1016/j.ymben.2019.03.009>.
- [32] Y. Lv, Y. Gu, J. Xu, J. Zhou, P. Xu, Coupling metabolic addiction with negative autoregulation to improve strain stability and pathway yield, *Metab. Eng.* 61 (2020) 79–88. <https://doi.org/10.1016/j.ymben.2020.05.005>.
- [33] B. Van den Bergh, T. Swings, M. Fauvart, J. Michiels, Experimental Design, Population Dynamics, and Diversity in Microbial Experimental Evolution, *Microbiol. Mol. Biol. Rev.* 82 (2018) 1–54. <https://doi.org/10.1128/mmbr.00008-18>.
- [34] D. Gresham, M.J. Dunham, The enduring utility of continuous culturing in experimental evolution, *Genomics*. 104 (2014) 399–405. <https://doi.org/10.1016/j.ygeno.2014.09.015>.
- [35] H. Bachmann, D. Molenaar, F. Branco Dos Santos, B. Teusink, Experimental evolution and the adjustment of metabolic strategies in lactic acid bacteria, *FEMS Microbiol. Rev.* 41 (2017) S201–S219. <https://doi.org/10.1093/femsre/fux024>.
- [36] Jef Huisman and Franz J. Weissing, Light-Limited Growth and Competition for Light in Well-

Mixed Aquatic Environments: An Elementary Mode, *Ecology*. 75 (1994) 507–520.

- [37] Q. Béchet, A. Shilton, B. Guieysse, Modeling the effects of light and temperature on algae growth : State of the art and critical assessment for productivity prediction during outdoor cultivation, *Biotechnol. Adv.* 31 (2013) 1648–1663.
<https://doi.org/10.1016/j.biotechadv.2013.08.014>.
- [38] E. Lee, M. Jalalizadeh, Q. Zhang, Growth kinetic models for microalgae cultivation : A review, *Algal Res.* 12 (2015) 497–512. <https://doi.org/10.1016/j.algal.2015.10.004>.
- [39] O. Bernard, F. Mairet, Modelling of Microalgae Culture Systems with Applications to Control and Optimization, in: *Microalgae Biotechnol. Adv. Biochem. Eng.*, Springer, 2015.
<https://doi.org/10.1007/10>.
- [40] J. Monod, The Growth of Bacterial Cultures, *Annu. Rev. Microbiol.* 3 (1949) 371–394.
<https://doi.org/10.1146/annurev.mi.03.100149.002103>.
- [41] C. Martínez, F. Mairet, O. Bernard, Theory of turbid microalgae cultures, *J. Theor. Biol.* 456 (2018) 190–200. <https://doi.org/10.1016/j.jtbi.2018.07.016>.
- [42] S. Aiba, Growth kinetics of photosynthetic microorganisms, in: *Microbial Reactions. Advances in Biochemical Engineering*, vol. 23. Springer, Berlin, Heidelberg, 1982: pp. 85–156.
https://doi.org/10.1007/3540116982_3.
- [43] S.F. Elena, R.E. Lenski, Evolution experiments with microorganisms: The dynamics and genetic bases of adaptation, *Nat. Rev. Genet.* 4 (2003) 457–469. <https://doi.org/10.1038/nrg1088>.
- [44] T. Leinonen, R.B. O’Hara, J.M. Cano, J. Merilä, Comparative studies of quantitative trait and neutral marker divergence: A meta-analysis, *J. Evol. Biol.* 21 (2008) 1–17.
<https://doi.org/10.1111/j.1420-9101.2007.01445.x>.
- [45] R.E. Lenski, Experimental evolution and the dynamics of adaptation and genome evolution in microbial populations, *ISME J.* 11 (2017) 2181–2194. <https://doi.org/10.1038/ismej.2017.69>.

- [46] S.E. Luria, M. Delbrück, Mutations of bacteria from virus sensitivity to virus resistance, *Genetics*. 28 (1943) 491 LP – 511. <http://www.genetics.org/content/28/6/491.abstract>.
- [47] G.N. Proctor, Mathematics of microbial plasmid instability and subsequent differential growth of plasmid-free and plasmid-containing cells, relevant to the analysis of experimental colony number data, *Plasmid*. 32 (1994) 101–130. <https://doi.org/10.1006/plas.1994.1051>.
- [48] P. Rugbjerg, N. Myling-Petersen, A. Porse, K. Sarup-Lytzen, M.O.A. Sommer, Diverse genetic error modes constrain large-scale bio-based production, *Nat. Commun.* 9 (2018) 787. <https://doi.org/10.1038/s41467-018-03232-w>.
- [49] R. Fischer, On the Dominance Ratio, *Proc. R. Soc. Edinburgh*. 42 (1923) 321–341.
- [50] S. Wright, Evolution in mendelian populations, *Genetics*. 16 (1931) 97–159.
- [51] P. A. P. Moran, Random Processes in Genetics, *Math. Proc. Cambridge Philos. Soc.* 54 (1958) 60–71.
- [52] G. V Barroso, A.F. Moutinho, J.Y. Dutheil, A Population Genomics Lexicon., In. Dutheil J. (2020) 3–17. https://doi.org/10.1007/978-1-0716-0199-0_1.
- [53] M.A. Nowak, *Evolutionary Dynamics: Exploring the Equations of Life*, Harvard University Press, 2006. <http://www.jstor.org/stable/j.ctvjghw98>.
- [54] S. Watanabe, Cyanobacterial multi-copy chromosomes and their replication, *Biosci. Biotechnol. Biochem.* 84 (2020) 1309–1321. <https://doi.org/10.1080/09168451.2020.1736983>.
- [55] L. Sun, H.K. Alexander, B. Bogos, D.J. Kiviet, M. Ackermann, S. Bonhoeffer, Effective polyploidy causes phenotypic delay and influences bacterial evolvability, *PLoS Biol.* 16 (2018) e2004644.
- [56] K. Zerulla, K. Ludt, J. Soppa, The ploidy level of *Synechocystis* sp . PCC 6803 is highly variable and is influenced by growth phase and by chemical and physical external parameters, *Microbiol.* 162 (2016) 730–739. <https://doi.org/10.1099/mic.0.000264>.

- [57] S. Liu, Sustainability and Stability, in: S.B.T.-B.E. (Second E. Liu (Ed.), Bioprocess Eng., Elsevier, 2017: pp. 871–947. <https://doi.org/10.1016/B978-0-444-63783-3.00015-0>.
- [58] D. Mattanovich, B. Gasser, H. Hohenblum, M. Sauer, Stress in recombinant protein producing yeasts, *J. Biotechnol.* 113 (2004) 121–135. <https://doi.org/10.1016/j.jbiotec.2004.04.035>.
- [59] H. Ling, W. Teo, B. Chen, S. Su, J. Leong, M.W. Chang, Microbial tolerance engineering toward biochemical production: from lignocellulose to products, *Curr. Opin. Biotechnol.* 29 (2014) 99–106. <https://doi.org/10.1016/j.copbio.2014.03.005>.
- [60] E. Sforza, S. Urbani, A. Bertucco, Evaluation of maintenance energy requirements in the cultivation of *Scenedesmus obliquus*: effect of light intensity and regime, *J. Appl. Phycol.* 27 (2015) 1453–1462. <https://doi.org/10.1007/s10811-014-0460-x>.
- [61] H.W. Kim, R. Vannela, C. Zhou, B.E. Rittmann, Nutrient acquisition and limitation for the photoautotrophic growth of *Synechocystis* sp. PCC6803 as a renewable biomass source, *Biotechnol. Bioeng.* 108 (2011) 277–285. <https://doi.org/10.1002/bit.22928>.
- [62] A. Cordara, A. Re, C. Pagliano, P. Van Alphen, R. Pirone, G. Saracco, F. Branco dos Santos, K. Hellingwerf, N. Vasile, Analysis of the light intensity dependence of the growth of *Synechocystis* and of the light distribution in a photobioreactor energized by 635 nm light, *Peer J.* 6 (2018) e5256. <https://doi.org/10.7717/peerj.5256>.
- [63] H.L. Macintyre, T.M. Kana, T. Anning, R.J. Geider, Photoacclimation of photosynthesis irradiance response curves and photosynthetic pigments in microalgae and cyanobacteria, *J. Phycol.* 38 (2002) 17–38.
- [64] C.P. Deblois, A. Marchand, P. Juneau, Comparison of Photoacclimation in Twelve Freshwater Photoautotrophs (Chlorophyte, Bacillariophyte, Cryptophyte and Cyanophyte) Isolated from a Natural Community, *PLoS One.* 8 (2013) e57139. <https://doi.org/10.1371/journal.pone.0057139>.

- [65] L. Straka, B.E. Rittmann, Dynamic response of *Synechocystis* sp. PCC 6803 to changes in light intensity, *Algal Res.* 32 (2018) 210–220. <https://doi.org/10.1016/j.algal.2018.04.004>.
- [66] L. Straka, B.E. Rittmann, Light-dependent kinetic model for microalgae experiencing photoacclimation, photodamage, and photodamage repair, *Algal Res.* 31 (2018) 232–238. <https://doi.org/10.1016/j.algal.2018.02.022>.
- [67] L. Straka, B.E. Rittmann, Light attenuation changes with photo-acclimation in a culture of *Synechocystis* sp. PCC 6803, *Algal Res.* 21 (2017) 223–226. <https://doi.org/10.1016/j.algal.2016.11.024>.
- [68] P.D. Sniegowski, P.J. Gerrish, Beneficial mutations and the dynamics of adaptation in asexual populations, *Phil. Trans. R. Soc. B.* 365 (2010) 1255–1263. <https://doi.org/10.1098/rstb.2009.0290>.
- [69] L. Perfeito, L. Fernandes, C. Mota, I. Gordo, Adaptive mutations in bacteria: High rate and small effects, *Science* 317 (2007) 813–815. <https://doi.org/10.1126/science.1142284>.
- [70] L.J. Jazmin, Y. Xu, Y.E. Cheah, A.O. Adebisi, C.H. Johnson, J.D. Young, Isotopically nonstationary ^{13}C flux analysis of cyanobacterial isobutyraldehyde production, *Metab. Eng.* 42 (2017) 9–18. <https://doi.org/10.1016/j.ymben.2017.05.001>.
- [71] E. Renshaw, *Modelling Biological Populations in Space and Time* (Cambridge Studies in Mathematical Biology), Cambridge University Press, 1991. <https://doi.org/doi:10.1017/CBO9780511624094>.
- [72] T. Székely, K. Burrage, Stochastic simulation in systems biology, *Comput. Struct. Biotechnol. J.* 12 (2014) 14–25. <https://doi.org/10.1016/j.csbj.2014.10.003>.
- [73] H. Li, L.A. Sherman, Characterization of *Synechocystis* sp. strain PCC 6803 and Δnbl mutants under nitrogen-deficient conditions, *Arch. Microbiol.* 178 (2002) 256–266. <https://doi.org/10.1007/s00203-002-0446-y>.

- [74] W. Du, J.A. Jongbloets, H. Pineda Hernández, F.J. Bruggeman, K.J. Hellingwerf, F. Branco dos Santos, Photonfluxostat: A method for light-limited batch cultivation of cyanobacteria at different, yet constant, growth rates, *Algal Res.* 20 (2016) 118–125.
<https://doi.org/10.1016/j.algal.2016.10.004>.
- [75] V.A. Portnoy, D. Bezdan, K. Zengler, Adaptive laboratory evolution — harnessing the power of biology for metabolic engineering, *Curr. Opin. Biotechnol.* 22 (2011) 590–594.
<https://doi.org/10.1016/j.copbio.2011.03.007>.

Tables and figures captions

Parameter	Assigned value	Reference
c_{\max}	0.223 h^{-1}	Fitted from data by [62]
k_s	$112 \text{ } \mu\text{mol photons m}^{-2} \text{ s}^{-1}$	Fitted from data by [62]
k_l	$748 \text{ } \mu\text{mol photons m}^{-2} \text{ s}^{-1}$	Fitted from data by [62]
k_d	0.00790 h^{-1}	[61]
ε	$0.160 \text{ m}^2 \text{ g}^{-1}$	Calculated from [67]
m	10^{-5} per generation	[69]
ρ	15 %, 30 %	[21,23,48,70]

Table 1. Parameters assigned to the model to simulate the dynamics of a photosynthetic retro-mutant sub-population of *Synechocystis* sp. PCC 6803.

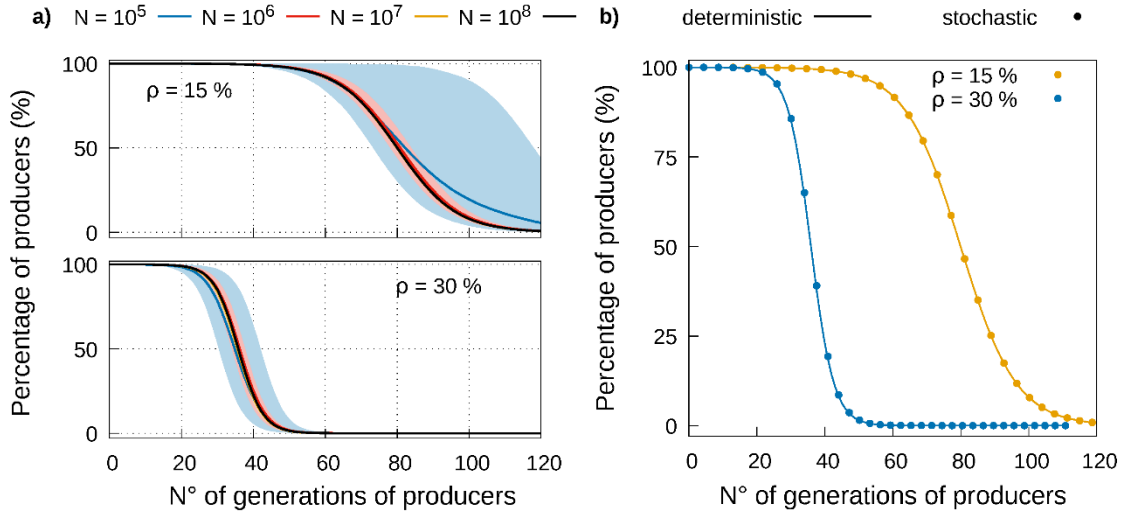


Figure 1. Trends of the percentage of producers with increasing number of generations of producers, calculated by setting the production burden to 15 % and 30 % and the mutation rate to 10^{-5} per generation. (a) Trend of the percentage of producers obtained with the stochastic model using different values of population size (N). Lines indicate the average values of up to 10 random Moran runs, whereas the shade areas cover from the minimum to the maximum value obtained at each generation and collapse to a line for the largest populations. (b) Trends of the percentage of producers obtained with the deterministic model and the stochastic model estimated with population size of 10^8 .

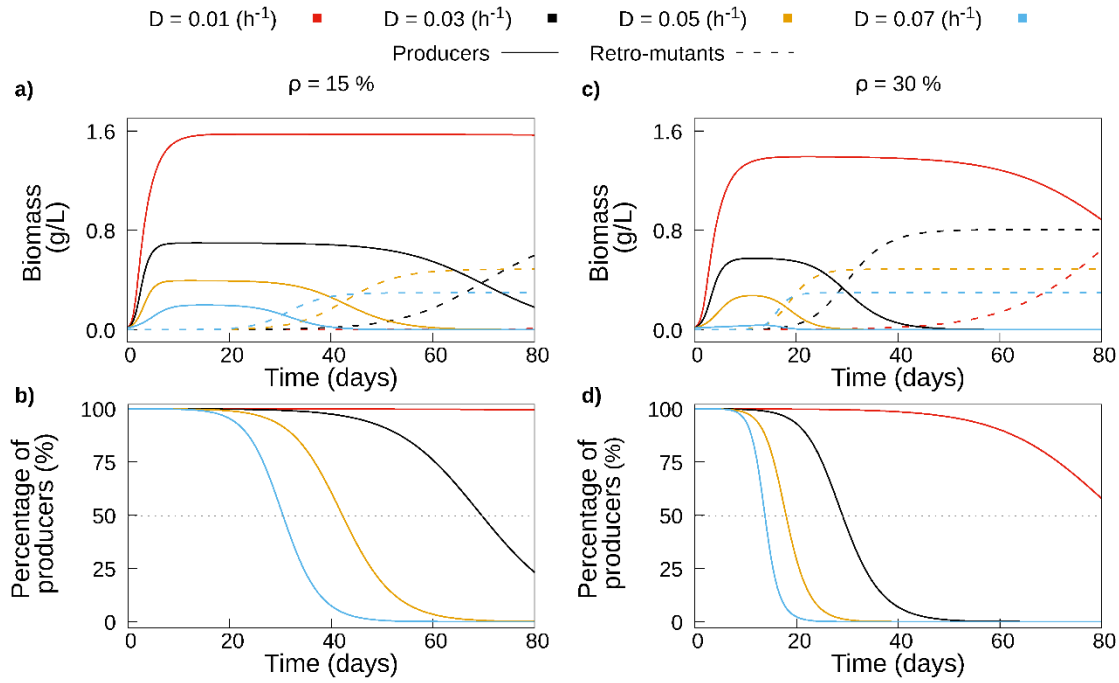


Figure 2. Simulations of population dynamics in a flat panel cultivation system operated in chemostat mode with different values of dilution rate (D). Trends of the biomass contribution of the producers and retro-mutants (a and c) and of the percentage of producers (b and d), calculated setting the production burden respectively to 15 % and 30 % and the mutation rate to 10^{-5} per generation.

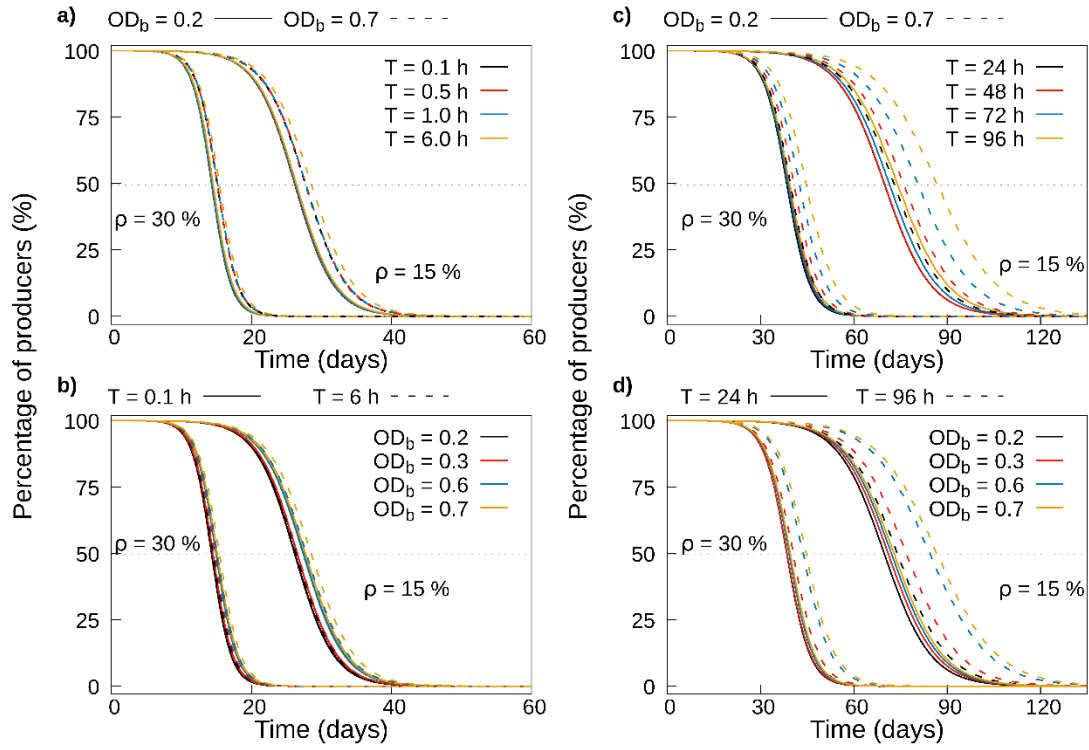


Figure 3. Simulations of population dynamics in turbidostat and serial batch transfer cultivation modes. Trends of the percentage of producers at varying T (**a** and **c**) and OD_b (**b** and **d**) in a flat panel operated in turbidostat mode (**a** and **b**) and in serial batch transfer mode in Erlenmeyer flask (**c** and **d**), calculated setting the production burden to 15 % and 30 % and the mutation rate to 10^{-5} per generation.

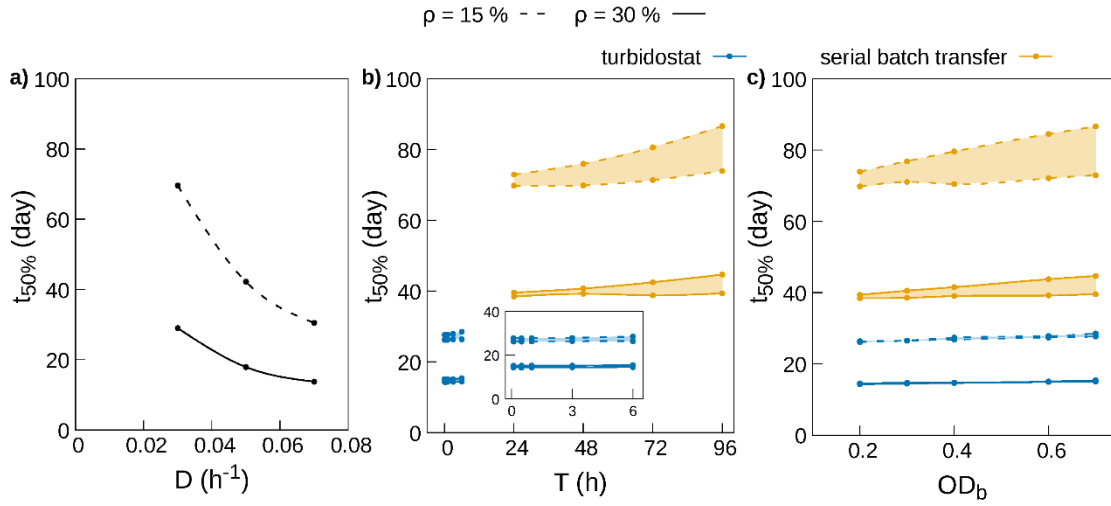


Figure 4. Trends of the time-instant ($t_{50\%}$) at which a drop to 50 % of the producers is observed in the different cultivation modes at different values of operative parameter D , T and OD_b . Trends of $t_{50\%}$ at increasing values of D in the chemostat mode (a), and at increasing values of T (b) and OD_b (c) in the turbidostat and serial batch transfer modes. In panel b, the shade areas between two lines comprise the trends of $t_{50\%}$ for the values of OD_b ranging between 0.2 (bottom line) and 0.7 (top line) for both cultivation modes; for the turbidostat mode, the shade areas collapse to a line and an inset shows an enlarged view of the results. In panel c, the shade areas between two lines comprise the trends of $t_{50\%}$ for the values of T ranging between 0.1 h (bottom line) and 6 h (top line) for the turbidostat mode, and between 24 h (bottom line) and 96 h (top line) for the serial batch transfer mode; for the turbidostat mode, the shade areas collapse to a line.

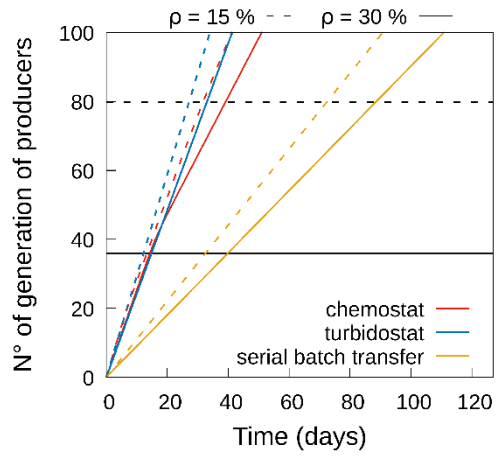


Figure 5. Comparison of the generation counting *versus* time in chemostat, turbidostat and serial batch transfer modes optimized for the shortest $t_{50\%}$. The horizontal dashed and solid lines indicate the $g_{p,50\%}$ respectively for production burden set to 15 % and 30 %.